Evaluation of the surface strength of glass plates shaped by hot slumping process

Laura Proserpio
Stefano Basso
Francesco Borsa
Oberto Citterio
Marta Civitani
Mauro Ghigo
Giovanni Pareschi
Bianca Salmaso
Giorgia Sironi
Daniele Spiga
Gianpiero Tagliaferri
Alberto D'Este
Roberto Dall'Igna
Mirko Silvestri
Giancarlo Parodi
Francesco Martelli
Marcos Bavdaz
Eric Wille

Evaluation of the surface strength of glass plates shaped by hot slumping process

Laura Proserpio,[a,*] **Stefano Basso,**[a] **Francesco Borsa,**[a] **Oberto Citterio,**[a] **Marta Civitani,**[a] **Mauro Ghigo,**[a] **Giovanni Pareschi,**[a] **Bianca Salmaso,**[a,b] **Giorgia Sironi,**[a] **Daniele Spiga,**[a] **Gianpiero Tagliaferri,**[a] **Alberto D'Este,**[c] **Roberto Dall'Igna,**[c] **Mirko Silvestri,**[c] **Giancarlo Parodi,**[d] **Francesco Martelli,**[d] **Marcos Bavdaz,**[e] **and Eric Wille**[e]

[a]INAF/Brera Astronomical Observatory, Via E. Bianchi 46, 23807 Merate, LC, Italy
[b]Università degli Studi dell'Insubria, Via Valleggio 11, 22100 Como, CO, Italy
[c]Stazione Sperimentale del Vetro, Via Briati 10, 30141 Murano, VE, Italy
[d]BCV Progetti, Via S. Orsola 1, 20123 Milano, MI, Italy
[e]ESTEC, European Space Agency, Keplerlaan 1, 2201 AZ Noordwijk, Netherlands

Abstract. Hot slumping technology is under development by several research groups in the world for the realization of grazing-incidence segmented mirrors for x-ray astronomy, based on thin glass plates shaped over a mold at temperatures above the transformation point. The performed thermal cycle and related operations might have effects on the strength of the glass, with consequences for the structural design of the elemental optical modules and, consequently, on the entire x-ray optic for large astronomical missions such as IXO and ATHENA. The mechanical strength of glass plates after they underwent the slumping process was tested through destructive double-ring tests in the context of a study performed by the Astronomical Observatory of Brera with the collaboration of Stazione Sperimentale del Vetro and BCV Progetti. The entire study was done on more than 200 D263 Schott borosilicate glass specimens of dimensions 100 mm × 100 mm and a thickness 0.4 mm, either flat or bent at a radius of curvature of 1000 mm through the pressure-assisted hot slumping process developed by INAF-OAB. The collected experimental data have been compared with nonlinear finite element model analyses and treated with the Weibull statistic to assess the current IXO glass x-ray telescope design, in terms of survival probability, when subjected to static and acoustic loads characteristic of the launch phase. The paper describes the activities performed and presents the obtained results. © *The Authors. Published by SPIE under a Creative Commons Attribution 3.0 Unported License. Distribution or reproduction of this work in whole or in part requires full attribution of the original publication, including its DOI.* [DOI: 10.1117/1.OE.53.8.085101]

Keywords: glass strength characterization; surface strength of glass; double-ring test; slumped plate; Weibull parameters; IXO x-ray telescope; ATHENA x-ray telescope.

Paper 140239P received Feb. 11, 2014; revised manuscript received Jun. 2, 2014; accepted for publication Jun. 26, 2014; published online Aug. 4, 2014.

1 Introduction

Hot slumping of thin glass foils is a very attractive technology under investigation by several groups for the realization of future segmented x-ray telescopes,[1–5] aimed at combining a large effective area with good angular and energy resolutions such as the ones planned for IXO-like or ATHENA-like missions.[6,7] The assembling of such telescopes will be based on a principle of hierarchical integration: single mirrors segments will be integrated into elemental modules, usually called an x-ray optical unit (XOU), then assembled and aligned in the flight mirror assembly (FMA) through intermediate azimuthal structures to reestablish the cylindrical symmetry of the nested telescope with a Wolter I (or a Wolter I approximation) optical design.[8] Slumping technology has already been successfully employed for the production of the NuSTAR telescope, launched in 2012,[9,10] which is able to deliver high image quality at a focus of 45 arcsec HEW.[11] Additional studies are currently ongoing both by American and European research groups to further expand the technology in terms of the achievable optical quality (the goal being 5 arcsec HEW).[12,13] The use of glass for the manufacturing of mirror segments, and possibly for

structural elements, ensures that these products meet the stringent mass requirements of space missions. However, this brittle material poses tight limits to the allowable stress level occurring during the entire life of the optical payload and requires a proper approach for the safety check during the design phases. Many different phenomena can simultaneously occur and determine the stress levels during the different steps of payload manufacturing and mission operation, such as stresses induced during the handling operation, transportation, ground testing, liftoff or thermal gradients, just to mention a few. Moreover, the strength of glass is not an intrinsic property of the material, but depends on the fabrication process and material history. The presence of flaws on the surface of the glass is the most relevant parameter, since flaws concentrate the stress and reduce the theoretical strength. The distribution of such microcracks, the stress distribution and the size of the stressed area, the residual internal stresses from production process, the fracture toughness, and the "static fatigue" phenomenon are all elements to be taken into account when looking for the strength parameter of glass components. The strength of a glass component can, therefore, only be defined by adopting a statistical approach based on experimental tests performed on specimens subjected to the same processes envisaged for the final parts, since each phase of their life could, in principle, induce different critical defects.

The activities described in the present paper represent one of the first steps in the analysis of this complex argument. A similar study was internally conducted at NASA in the frame of the Constellation-X mission;[14] compared to that this work adds a further step in the analyses of results which may give the possibility of also applying experimental data to the effective stress distribution on the mirror modules and not only to the stress distribution recorded during tests. These activities have been realized in the frame of a study supported and coordinated by ESA and led by the Astronomical Observatory of Brera with the collaboration of other institutes such as MPE and small enterprises such as BCV-Progetti (Milano, Italy), ADS-International (Lecco, Italy), and Media Lario International (Bosisio Parini, LC, Italy).[15] Even though the baseline for the realization of the IXO mirrors was represented by the so called "Silicon Pore Optics" technology, investigated so far by ESA in collaboration with the Cosine company[16] and currently adopted for the ATHENA mirrors,[17] the study is continuing with the scope of using the glass technology for the x-ray mirrors of other future missions.

During the last 5 years, several prototypes have been realized[18] that show the potential of the INAF-OAB slumping and integration approach, and a design for the complete IXO x-ray optical payload made by glass has been carried out.[19] One of the main scopes of this present study was to gain an experimental number to demonstrate the goodness of the hypothesis on which this current design is based.

The paper focused on the evaluation of the surface strength of the thin glass plates shaped by the hot slumping process that are used for mirror segments: their strength has been characterized by the evaluation of the Weibull distribution, a classical statistic approach adopted to check the strength of brittle materials. The Weibull parameters have been evaluated by fitting experimental data coming from destructive double-ring tests on slumped plates and have been employed for the check of the current IXO telescope

design. The paper is organized into five main sections according to the flow of activities sketched in Fig. 1.

2 Slumped Samples Realization

The statistical nature of the Weibull approach required the realization by thermal slumping of a large number of glass samples, prepared following a process well representative of the final production of the x-ray segmented mirrors for the flight modules. The entire production chain comprises several steps encompassing the procurement and selection of glass foils, their cutting to the required dimension for pursuing the hot shaping process, their cleaning, the realization of the thermal cycle, the postcutting to the final dimensions of the x-ray mirror segments, their coating with a reflective layer, and the final integration into the XOU. If these steps are carried out in different locations, packaging and shipment also have to be considered. All these production steps could, in principle, affect the strength parameters of the final realized mirror. It is worth noting that further investigations currently ongoing to improve the performances. The current procedures might, therefore, be subjected to changes as the result of the optimization and industrialization of the process. Since the current available laboratory setup involves several steps that are still realized manually and with a lower degree of automation than is expected to be available during mass production, the results obtained are representative of the current best knowledge of the process and should be considered conservative from the point of view of the production of samples.

2.1 Hot Slumping Process with Pressure Assistance

Different slumping processes exist: almost all share the basic idea of forming a thin glass mirror by shaping it over a mold through the application of a suitable thermal cycle that changes the viscosity properties of the glass, allowing it to deform in order to assume a desired shape. Depending on the side of the forming mirror that comes in contact with the mold, two approaches are possible: the direct approach, in which the optical surface of the mirror comes in contact with the mold during the process, and the indirect approach, in which contact happens on the back side.[20] The deformation of glass could take place only under its own weight (that is, by gravity) or can be actively supported by the application of additional external forces. The particular process considered in the present work is known as direct hot slumping with pressure assistance,[21] and is a direct approach characterized by the active application of pressure to help the glass reach full contact with the mold surface, ensuring the absence of mid-frequencies deformations (in the range between a few millimeters and a couple of centimeters) that degrade the optical performances. During the course of the activities, many improvements have been made in the hot slumping technology with pressure assistance. In particular, a new method for pressure application has been developed: while the original approach developed at OAB makes use of a thin metal membrane for applying pressure on the glass plate being shaped to force it into full contact with the mold, the new approach allows for the application of pressure directly on the glass plate without intermediate materials.[22] In this way, it is possible to avoid random local deformations and surface damage introduced by the metal pressing membrane that have detrimental effects
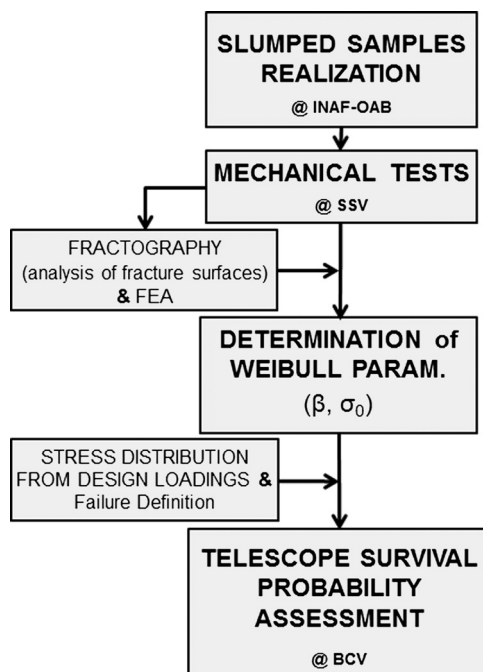
SLUMPED SAMPLES REALIZATION
@ INAF-OAB

MECHANICAL TESTS
@ SSV

FRACTOGRAPHY
(analysis of fracture surfaces)
& FEA

DETERMINATION of WEIBULL PARAM.
(β, σ_0)

STRESS DISTRIBUTION
FROM DESIGN LOADINGS **&**
Failure Definition

TELESCOPE SURVIVAL PROBABILITY ASSESSMENT
@ BCV

Fig. 1 Flow of the activities presented in the paper.

both on the mirror segments' shape, meaning optical performances, and on strength. In both cases, the entire process of slumping is realized inside a stainless steel muffle for thermal and cleaning reasons: in the first case, the muffle is divided in two separate volumes by a 25-μm-thick metal membrane, whereas in the second case the glass foil itself acts as a membrane to separate the muffle in two different chambers. In this way, a differential pressure can be established.

2.2 Production of Samples

Accordingly, two main methods have been employed for the production of samples for the present study, i.e., the slumping with or without the use of a metal pressing membrane (see Figs. 2 and 3). The rationale behind the decision of producing the specimens in the two ways was twofold. There was a temporal reason, since at the beginning of activities, the new method for pressure application was not completely developed and the baseline was still considered to be the original one with the metal membrane. Furthermore, this decision provided an opportunity for performing a quantitative comparison of the two approaches with respect to the foil
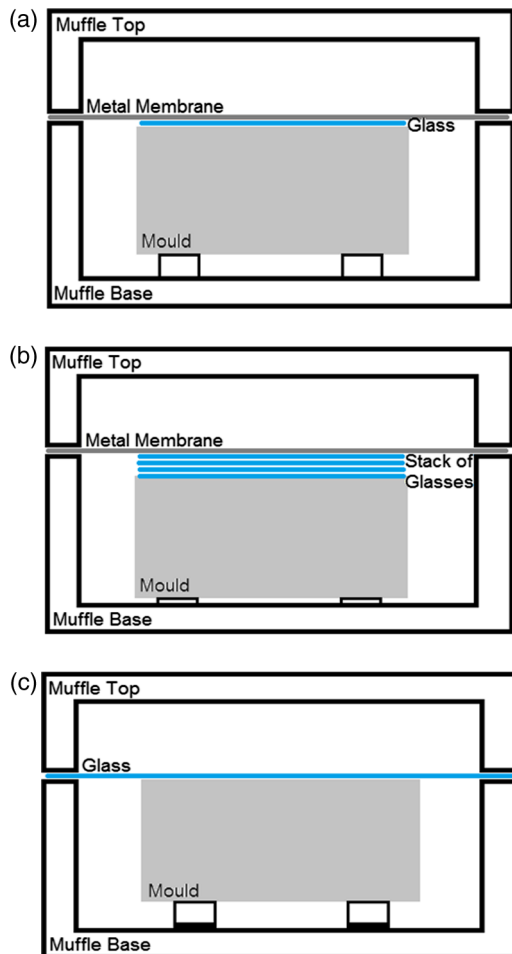
Fig. 3 Comparison between the two INAF-OAB approaches for pressure application during slumping. (a) The application of pressure is realized through the use of metallic membrane. (b) The glass foil itself acts as a membrane allowing for pressure application.

strength characteristics. In order to speed up the specimens' production, a stacking concept was initially considered: in every run, four glass foils were slumped together in a stack, applying the pressure only on the last foil of the stack. To avoid their mutual sticking, sheets of the same material as the metal pressing membrane or boron nitride (BN) layers deposited on the glass surface have been interposed between them with the hypothesis that this situation was representative of the glass back surface condition, which during slumping comes in contact with the pressing membrane. However, after a number of tests, this solution introduced spurious effects, mainly related to the cleaning issue, to the intrinsic structure of the thin membrane and to the dusty nature of the BN layer. Meanwhile, the new pressure application method has been developed, and the stacking concept of foils within the muffle was no longer representative: in the new process, the back side of the glass foil being shaped is free, i.e., without contact with any external material. For this reason, the last samples have been produced by slumping each glass plate at a different time: this slowed down the samples' production and introduced a delay into the original agenda of activities, but was fundamental for obtaining reliable data.

In total, 42 slumping cycles have been carried out for the production of the more than 200 specimens. They have all been prepared using the thermal-pressure cycle reported in Fig. 4: after a first heating-up ramp at ~60°C/h, the maximum temperature of 570°C is maintained for 2 h before starting the cooling phases, which are divided into three steps. The first cooling phase is at ~3°C/h, from T_{max} up to $T_{annealing}$ (557°C) and, after a second plateau, the others are carried out at ~5 and ~10°C/h. The 1-h holding at the annealing temperature guarantees the relaxation of

Fig. 2 Schematics of the slumping approaches followed for the production of samples considered in this study: (a) Pressure application through metal membrane; (b) stacking concept to speed up the production by slumping several glass plates at a time. Between the glass foils in the stack, metallic or BN layer has been used as antisticking (not shown in the schematic picture); and (c) pressure application directly on the glass plate, without any intermediate material.
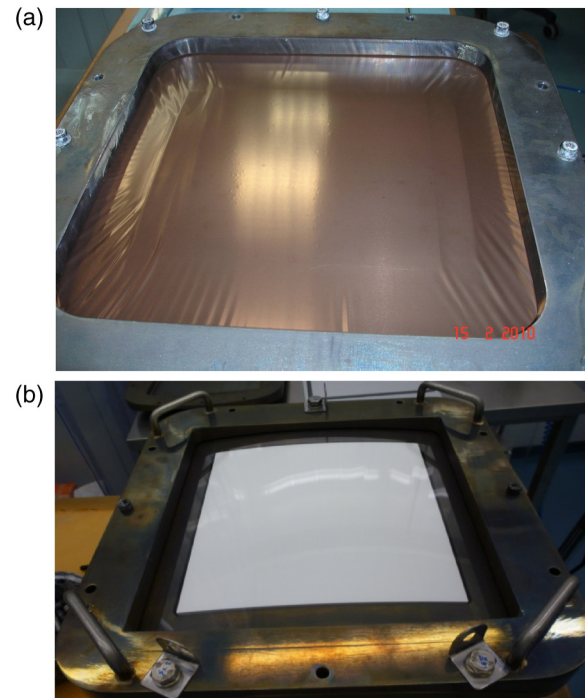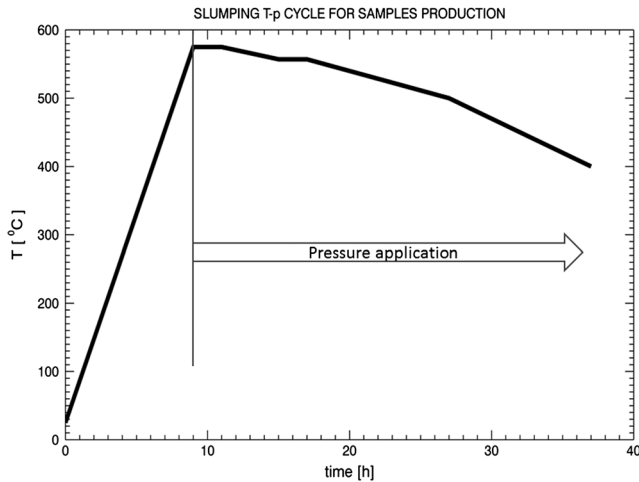
Fig. 4 Temperature-pressure cycle used for the realization of all borosilicate D263 samples on Zerodur K20 mold.

major stresses inside the glass. After the controlled cooling phase, the oven is switched off and freely cools down to room temperature. A pressure of 50 g/cm^2 is applied upon reaching the highest cycle temperature and is maintained until the oven is opened.

The samples' realization has been performed using the same materials as planned for IXO mirror manufacturing and following all related phases (except for the reflective layer deposition and integration steps) in keeping with the best current knowledge of the process. All specimens are made of borosilicate glass type D263 with a thickness 0.4 mm and are produced by Schott and slumped over a Zerodur K20 mold. These materials represent the baseline choice at the moment of writing: in particular, the glass type is already used for space applications (e.g., NuSTAR)

and is preferable with respect to other thin glass foils available on the market because of its relatively low characteristic temperatures. The Zerodur K20 glass-ceramic material used for the mold offers a great advantage in that it does not need an antisticking layer to prevent the adhesion of the D263 foils during the thermal cycles. One major drawback of this coupling of materials is represented by their not-perfect matching of the coefficients of thermal expansion, a problem that can be partially compensated for by adopting the low cooling down rate. All specimens are slumped in bigger foils and then cut to the dimensions of $100 \text{ mm} \times 100 \text{ mm}$ required for the strength tests. The cutting is performed with CO_2 laser technology, realized through the services of MDI Schott, Mainz, Germany.

The majority of specimens are flat because of the knowledge of the double-ring test procedure and the consequent reliability in data analyses; some of them are cylindrical, with a radius of curvature of 1000 mm, representative of an intermediate mirror segment in the current optical design of the IXO telescope.

2.3 List of Samples Realized for the Present Study

Table 1 reports a summary of all realized specimens: they have been divided into different sets according to the specific procedure followed for their production and to the surface side that has been tested. In principle, the two surfaces of a slumped glass are different because of their different kinds of contact during the shaping process: the optical surface, in fact, experiences contact with the polished surface of the mold, while the back surface comes in contact with the metal pressing membrane (for the original approach) or does not experience contact at all (in case of the new slumping approach). While the specimens produced with the original approach have been tested on both surfaces, specimens produced with the new approach (sets AIR-P and AIR-C) have

Table 1 Summary of the realized and tested samples: they were all made of glass-type D263 slumped on Zerodur K20 mold and had dimension of $100 \text{ mm} \times 100 \text{ mm}$ with thickness of 0.4 mm. All samples were CO_2 laser cut at their edges after slumping.

Set	#	Shape	Slumping realization	Tested surface[a]	Notes
TQ	49	Flat	n.a.	Both[b]	Samples as delivered by vendor, give the maximum theoretical strength for untreated glass.
STEEL	31	Flat	Old approach, in stack with interposed metal membrane	Back	Tested on back surface that has lower strength because of its contact during slumping with metal pressing membrane or BN layer. Presence of imprinting of the microstructure of the antisticking interlayers.
GLASS	45	Flat	Old approach, in stack with interposed BN layer	Back	
MOULD$_1$	16	Flat	Old approach, stack configuration	Optical	Obtained by the same experimental tests of sets STEEL and GLASS, considering the lower glass in the stack that during slumping was in contact with the mold.
MOULD$_2$	18	Flat		Optical	
AIR-P$_{air}$	28	Flat	New approach: pressure directly applied on the free-back surface of glass	Back	All tested on the back surface; however, depending on the side where the failure occurred, they are considered separately representative of the optical or back surface.
AIR-P$_{mold}$	30	Flat		Optical	
AIR-C$_{air}$	32	Cylindrical		Back	
AIR-C$_{mold}$	17	Cylindrical		Optical	
Total	266				

[a]*Back surface* means the surface of the glass that during the slumping process did not come in contact with the mold and were in contact with metal membrane or boron nitride (BN) interposed antisticking layer for STEEL and GLASS or was not in contact with anything for sets AIR-P and AIR-C.
[b]*Both* apply in the considered hypothesis that the surfaces of the glass are exactly the same when it is delivered by the vendor given the symmetry of the down-drawn production process.

been tested just on their back surface, since the side in contact with the mold should, in principle, have the same behavior as that obtained with the original slumping process. However, during tests realizations, a significant number of failures have been registered on the optical side, in spite of the lower tensile stress level induced by test setup. This happened because the contact of the glass foils with the mold at the optical side somehow reduced the glass strength with respect to the back side. For this reason, depending on the side where the failure occurred, these specimens are identified with two set names and are considered representative, respectively, of the strength of the optical and of the nonoptical sides. A further set composed of not-slumped plates was also considered for comparison reasons: they were characterized in order to provide a reference maximum value for glass strength that could be maintained after the slumping process. This value represents the best upper limit for untreated glass and is subject to an unavoidable (though reducible with optimized operations) decrease during each phase of glass life.

As reported in Table 1, the number of specimens for each set is variable and not uniform: this is mainly due to time constraint reasons and to a few breakages experienced during the cutting or shipment operations. On average, the number of samples for each set is around 30 units. In spite of the fact that this number is quite small for the derivation of statistical data, we believe that this preliminary analysis was very useful in allowing us to identify weak points, fix some process procedures, and develop experience in testing slumped glass strength for implementing the obtained data in the structural design process. To our knowledge, it represents the only analysis of its kind performed to date for thin slumped foils to be used in space experiments.

3 Mechanical Tests Realization

The structural use of glass raises the issue of determining its failure strength. This implies reliable statistics regarding failure probability and the experimental determination of probability distribution parameters. The four-point bending test and ring-on-ring (RoR) test[23–26] are normally used for assessing whether glass plates comply with the pertinent product standard. A review of these test methods had been conducted in the past at Stazione Sperimentale del Vetro (SSV);[27] namely, the influence of the area under tensile stress and the effect of the nonuniform stress field were the subject of focus on in order to estimate the material's Weibull parameters. Since no specific standard is available for glass plates of 0.4-mm thick, existent testing method standards were taken only as a guideline. Due to the broad strength data spread usually observed for brittle materials, EN 1288 standard prescribes using a large but unspecified number of specimens when the testing purpose is to determine the characteristics or design bending strength of glass plates. As experimental data have to be statistically evaluated, the sample size for each tested set cannot be fewer than 30 specimens.[28]

Considering one testing method, we can say that the smaller the loaded area, the higher the average strength of the sample, because the probability of finding critical defects correspondingly decreases. Therefore, the size of the loaded area is a fundamental element when evaluating the experimental failure probability with different tests and geometries. Generally, using small loaded areas results in great strength

value variability and it usually brings an overestimation the mechanical resistance of glass. Hence, testing small specimens is recommended for comparison purposes only. Nevertheless, using physically based statistical fracture methods for the evaluation of breakage probability allows for the correlation of results obtained with similar stress fields, but on different areas,[29] as long as the effective Weibull area does not prove to be less than 100 mm^2.[30] Tests carried out using equal-sized loading areas subjected to different stress fields (e.g., uniaxial or biaxial tensile stress field) bring about different average strengths, i.e., higher failure stresses are observed under uniaxial stress fields. This is due to the crack's plane orientation relative to the principal stress directions: the crack-opening stress for a surface flaw not orthogonal to the uniaxial stress field is lower than the maximum principal stress, and the probability of unstable crack propagation is reduced. Therefore, the failure probability increases for biaxial stress fields in which more crack orientations may prove to be critical.

Based on the previous observations, the importance of linking experimental strength data to the pertinent testing method and to the size of the loaded area becomes evident. Therefore, in order to evaluate the mechanical strength of the developed glass foil samples, ad-hoc RoR tests were carried out at SSV laboratories in Murano (Venezia, Italy).

3.1 Experimental Setup

During a coaxial double-ring test, the specimen rests on a bearing ring on the testing machine and an increasing load is applied perpendicularly to its upper surface by means of a second ring until the specimen fails. An electrostatic 3M polymeric film (approximately 100-μm thick) was applied on the upper surface of the specimens in order to keep the glass fragments together on failure, thus making the fracture analysis easier by allowing the experts to trace the fracture origin (position where the fracture began) without affecting the test results. For flat specimens, a bearing toroid-ring with a radius of 45 mm and a loading toroid-ring with a radius of 30 mm (configuration R45-30, according to norm UNI-EN 1288:2001) were employed. For cylindrical specimens, an ad-hoc double-ring test was developed. The curved specimens were tested with a modified R45-14 configuration (i.e., having a bearing ring with a radius of 45 mm and a loading ring with a radius of 14 mm) in order to generate a biaxial stress field inside curved specimens while minimizing tensile stresses near the edges or constraints. The bearing ring was machined in order to follow the shape of the glass segment under testing and, at least at the beginning of the test, a perfect contact with the curved specimen was guaranteed. The torus shape of the loading ring was not modified, but its radius was reduced so that the distance between the loading ring and the glass surface was lower than the thickness of the electrostatic film applied on the upper surface (i.e., facing-up surface, the one in contact with the loading ring) of the specimens. A specific metallic template was designed for exact positioning of the curved specimens on the testing machine without interfering with the test implementation (see Fig. 5). Their concavity was placed upward, so that the nominal surface under test was the back one. All tests were performed in displacement control by means of an INSTRON-4411 dynamometer (maximum load 5 kN, resolution 0.1 N up to 400 N), with the

Fig. 5 **Fig. 5** Double-ring test configuration used for curved samples. The support and loading rings are clearly visible. The square element surrounding the support ring is used as a template for samples alignment on the machine and does not interfere with the test.

crossbar's displacement velocity of 1.39 mm/ min (flat sample case) or 0.5 mm/ min (curved sample case), corresponding to a stress increment in the samples of ∼2 MPa/s.

3.2 Data Collection

Load and displacement data were collected for each specimen. The slenderness of the specimens resulted in geometric nonlinearity, which prevents the application of analytical expressions. Consequently, three-dimensional nonlinear finite element model (FEM) analyses of both testing apparatuses (i.e., RoR for flat specimens or RoR for cylindrical specimens) were required for determining the actual stress field inside each specimen at breakage and, in particular, the breakage stress at the failure origin. Finite element analysis (FEAs) proved that the radial and circumferential (or tangential) stresses evocated in the specimen by the external load are not uniform nor equal to each other on the loading area (nonequibiaxial stress filed); moreover, high tensile stresses are also present on the upper surface of the specimens. For flat specimens: on the face-down surface, the radial stresses are greater than the tangential stresses and reach their maximum value at about 30 mm from the specimen's center, i.e., beneath the loading ring (see Fig. 6); on the face-up surface, the maximum tensile stress is reached by the radial stress at 45 mm from the center, in correspondence to the bearing ring, along the specimen's diagonal (see Fig. 7). In the same vein, for cylindrical specimens: on the face-down surface, the radial tensile stresses are greater than the tangential ones (except in the center where their values are comparable) and increase from the sample's center up to the loading ring: on the face-up surface, the maximum
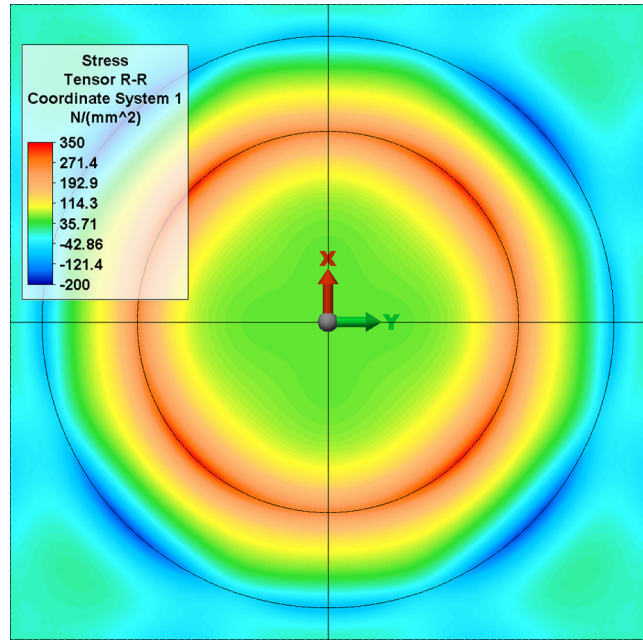

Fig. 6 Radial stress field from FEM simulation on the lower surface of flat specimens, beneath a 600-N load; the radial stresses reached their maximum value in correspondence of the loading ring.

tensile stresses are in the radial direction, located at the bearing ring near the sample diagonals.

To locate the failure origin, fractographic analyses were carried out on the specimens (except those that failed at higher loads and whose fragmentation prevented us from performing this analysis) and confirmed that the failures started where FEA identified the highest tensile stresses, as shown in Figs. 8 and 9. The fractographic analyses have been conducted by optical inspection of high-resolution images taken by an Olympus SZX12 stereo-microscope (up to 90× magnification). For all specimens of the sets TQ,
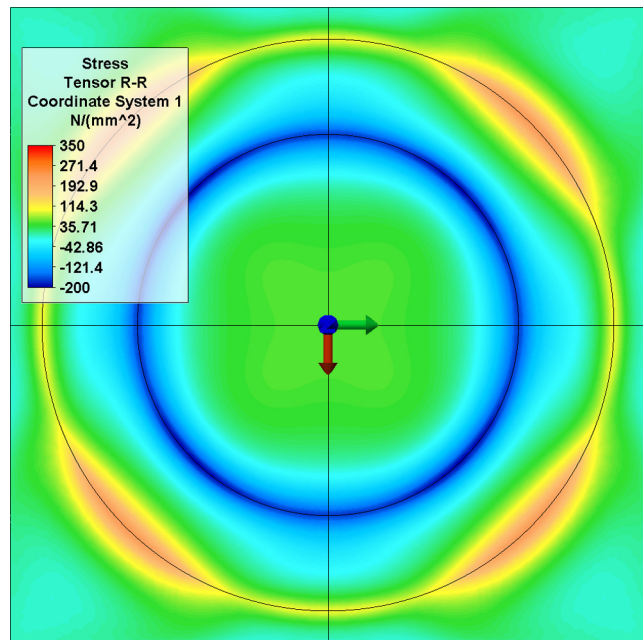

Fig. 7 Radial stress field from FEM simulation on the upper surface of flat specimens, beneath a 600-N load; the maximum tensile stress is reached by the radial stress at 45 mm from center, along diagonal.

Fig. 8 Typical fracture pattern for failures in flat specimens started at the lower (facing-down) surfaces.

Fig. 9 Typical fracture pattern for failures in flat specimens started at the upper (facing-up) surfaces.

Fig. 10 Fracture origins on samples AIR-P (flat specimens). The two circles represent the bearing-ring position (bigger circle) and the loading-ring position (smaller circle).

Fig. 11 Fracture origins on samples AIR-C (cylindrical specimens). The two circles represent the bearing-ring position (bigger circle) and the loading-ring position (smaller circle).

STEEL, GLASS, and MOULD, the fracture originated from the lower (face-down) surface (as expected from test configurations), and for the sets AIR-P and AIR-C, the breakage started from the upper (face-up) surface in 60 and 35%, respectively (as shown in Figs. 10 and 11), due to the surface strength depletion caused by the mold.

For some specimens slumped in a stack, the fracture analyses showed defects on the glass surface which was in contact with other material during the forming process, i.e., the mold surface, the metal pressing membrane, or one of the other glass foils in the stack (see Fig. 12). Typically, fractures that originated from these defects are ascribable to the slumping process and related phases (handling, cutting, and cleaning). There was no evidence of such defects on the as-delivered specimens (set TQ). For sets AIR-P and AIR-C, the fracture analysis of specimens that had
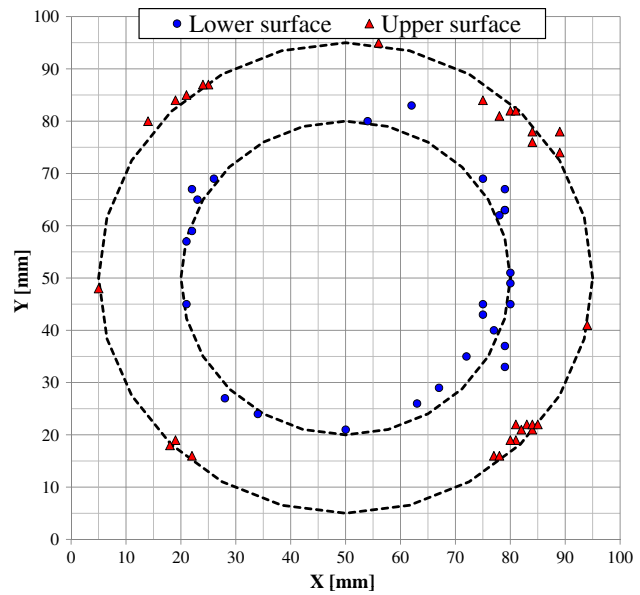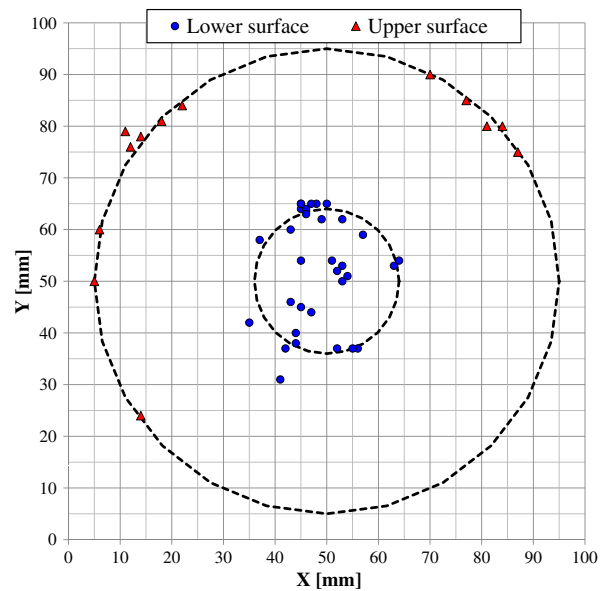
broken at the lower loads did not evidence the presence of particular surface defects close to the fracture origin [see Fig. 13(a)]. This demonstrates that the heavy defects observed on stack-slumped specimens were eliminated. Some secondary effects need to be more well analyzed. One possible explanation is related to the crystalline structure of the mold material (Zerodur K20), characterized by the presence of crystal grain inside an amorphous matrix. These crystals cause imprinting on the glass contact surface, both directly or because they make cleaning harder. Better cleaning and glass strengthening methods should help in reducing the impact of these flaws: at the time of writing, the use of
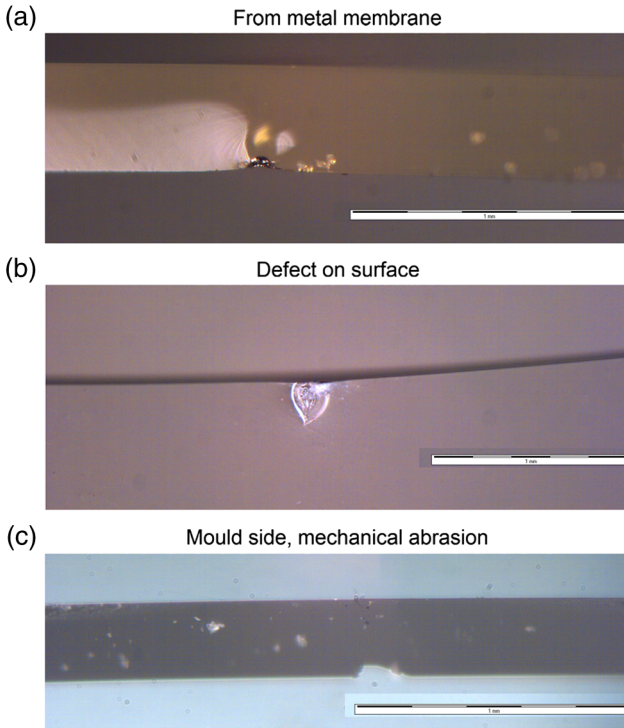
(a)

From metal membrane

(b)

Defect on surface

(c)

Mould side, mechanical abrasion

Fig. 12 The fractures origin generally from defects on the glass surface, e.g., (a) defect generated by the contact with the metal pressing membrane; (b) defect on the back surface probably related to handling issue; and (c) mechanical abrasion found on the side of the glass in contact with the mold.

lacquer to planarize the slumped glass surface is being analyzed.[31] On the back surface of some specimens of sets AIR-P$_{air}$ and AIR-C$_{air}$, a contamination of small metallic grains was found [see Fig. 13(b)]; its origin is due to the setup used for slumping that employed a stainless steel plate to shield the glass and mold from the direct heating of the electrical resistances in the oven in order to reduce
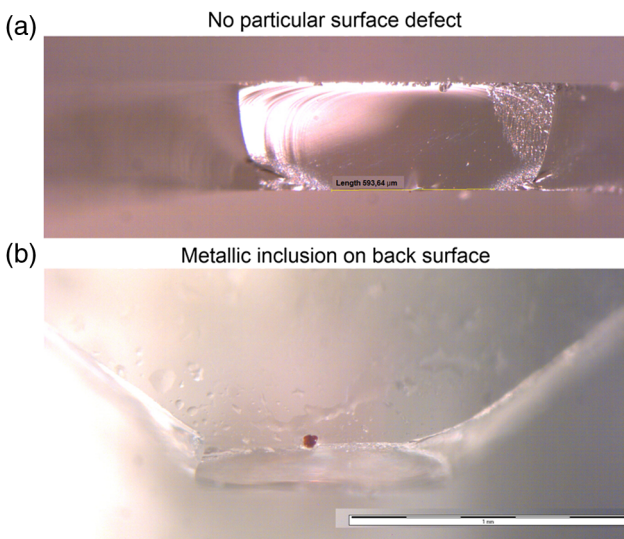
(a)

No particular surface defect

(b)

Metallic inclusion on back surface

Fig. 13 Area of fracture origins for two samples of set AIR-P: (a) No evident surface defects on the optical surface; and (b) metallic inclusion on the back surface, due to nonoptimal cleaning of a muffle cover in the oven.

minimum thermal gradients. This element was positioned over the muffle at the very last step of the process preparation just before closing the oven. A better control of the cleaning of this element will remove this contamination, which does not represent a critical issue.

4 Glass Weibull Parameters Determination

The mechanical resistance of glass is closely related to the characteristics of the flaws present on its surface (density, distribution, and orientation of the superficial cracks). Thus, glass strength measurements are strongly dependent on the testing procedure through the actual size of the loading area (different areas have different probabilities of finding critical cracks) and the ensuing stress field (the probability that the crack orientation will differ from principal stress directions). For a proper interpretation of glass fracture probability, physically based statistical fracture theories were developed[27,32–37] that, starting from Weibull's weakest link theory,[38] allow us to take into account the influence of the extent of the loading area and the actual stress field.

A statistical analysis of the failure probability data collected during the tests allowed the evaluation of the Weibull parameters that describe the mirror plates' strength. To evaluate the fracture probability within a multiaxial stress field, the simplest fracture criterion was used: namely, fracture mode I. For brittle materials like glass, this demonstrates a high level of concordance with experimental data:[27] once the existing surface flaws have been assimilated to flat cracks, the fracture expands when stress occurs in an orthogonal direction to the crack, surpassing the corresponding critical stress for mode I, σ_{Ic} (resistance of a crack placed orthogonally to the uniaxial stress). According to Weibull's formulation, the average number of cracks in unit areas with mechanical resistance less than σ_{Ic} can be expressed as

$$N(\sigma_{Ic}) = \left(\frac{\sigma_{Ic}}{\sigma_0}\right)^{\beta}. \tag{1}$$

The parameters β (module) and σ_0 (reference resistance) depend on the fracture toughness of the material and statistical properties regarding the distribution of the crack's dimensions on the surface.

Assuming that the specimens are under plane stress, if we hypothesize that for surface cracks, all directions contained in angle π have the same chance of being present, the fracture probability for homogeneous defectiveness is derived from

$$P = 1 - \exp\left[-\int_A \frac{1}{\pi} \int_\omega N(\sigma_{Ic} = \sigma_\perp) d\omega \, dA\right], \tag{2}$$

where A is the superficial area under tensile stress and $\sigma_\perp$ is the tensile stress that is orthogonal to the crack in an arbitrary direction.[39]

Expressing $\sigma_\perp$ as a function of the principal stresses

$$\sigma_\perp = [\sigma_1 \cdot \cos^2(\psi) + \sigma_2 \cdot \sin^2(\psi)]$$
$$= \sigma_1 \cdot [\cos^2(\psi) + r_2 \cdot \sin^2(\psi)], \tag{3}$$

we can write Eq. (2) as follows:

$$P = 1 - \exp\left\{-\int_A \left[\frac{1}{\pi}\int_\psi \left(\frac{\sigma_\perp}{\sigma_0}\right)^\beta \mathrm{d}\psi\right]\mathrm{d}A\right\}$$

$$= 1 - \exp\left[-\int_A \left(\frac{C \cdot \sigma_1}{\sigma_0}\right)^\beta \mathrm{d}A\right], \quad (4)$$

where ψ is the angle between the projection of the crack's normal on plane σ_1-σ_2 and the direction σ_1 and C is the coefficient that takes into consideration the multiaxial nature of the actual stress field ($C < 1$ in case $\sigma_1 \neq \sigma_2$) calculated as follows:[40,41]

$$C = \left\{\frac{2}{\pi} \cdot \int_0^\alpha \left[\cos^2(\psi) + \frac{\sigma_2}{\sigma_1} \cdot \sin^2(\psi)\right]^\beta \mathrm{d}\psi\right\}^{1/\beta}$$

$$\alpha = \frac{\pi}{2} \qquad \text{for } \frac{\sigma_2}{\sigma_1} \geq 0 \qquad (5)$$

with

$$\alpha = \arctan\sqrt{-\left|\frac{\sigma_1}{\sigma_2}\right|} \quad \text{for } \frac{\sigma_2}{\sigma_1} < 0 \;.$$

Once the Weibull parameter β is known, the failure probability can be expressed as a function of the maximum stress reached on the surface of the specimen under testing (σ_{max}), taking into account the effective area (S_{eff}) which represents the superficial area that, if subjected to a uniform equibiaxial stress field equal to the maximum stress, would show the same failure probability as the actual stress field

$$P = 1 - \exp\left[-\int_A \left(\frac{C \cdot \sigma_1}{\sigma_0}\right)^\beta \mathrm{d}A\right]$$

$$= 1 - \exp\left[-\left(\frac{\sigma_{max}}{\sigma_0}\right)^\beta \cdot S_{eff}\right]. \quad (6)$$

$$S_{eff} = \frac{\int_A (C\sigma_1)^\beta \mathrm{d}A}{\sigma_{max}^\beta}. \quad (7)$$

The breakage load data and the ensuing principal stresses obtained from the pertinent numerical model were used to determine the Weibull parameters of the glass surface (module, β, and reference strength, σ_0) by best fitting of the experimental failure probability for each sample set. For this purpose, an ad-hoc iterative algorithm based on the maximum likelihood method, as suggested by the ASTM C 1239-06A standard,[42] was implemented in MATLAB R2012b. Surface strength censoring caused by face-up breakages in the AIR-P and AIR-C datasets was also accounted for.

The step-by-step procedure for the iterative algorithm is as follows:

1. Guess a value for the module, β^*.
2. Considering the maximum and intermediate principal stress fields evocated on the specimen subjected by each experimental breakage load, calculate the pertinent products $(\sigma_{max} \cdot S_{eff}^{1/\beta})^*$.
3. Calculate the Weibull parameters (β, σ_0) using the maximum likelihood method on the $(\sigma_{max} \cdot S_{eff}^{1/\beta})^*$ dataset.
4. If $|\beta^* - \beta| > \varepsilon$, designate the module β obtained above as the new value of β^* and return to step (2) then repeat steps (2) and (3) until convergence is achieved.
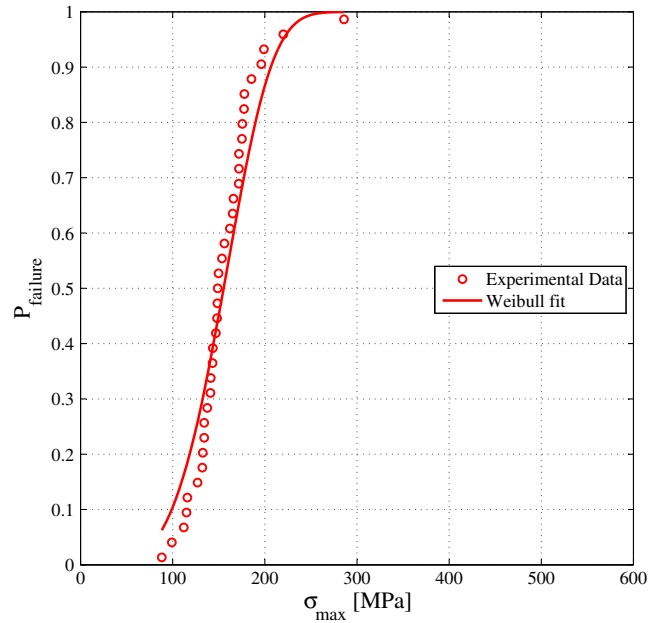

Fig. 14 Example of how the Weibull curve fits the experimental data: the particular case refers to MOULD set.

Figure 14 shows the Weibull curve fitting of the failure probability for the MOULD set of experimental data as a function of the maximum stress. The values of the Weibull module and the characteristic parameter obtained by the analysis of the data (see Refs. 43 and 44) are summarized in Table 2, together with the minimum breakage stress recorded for each sample. These minimum strength values cannot be directly applied to glass plates different in size or load configuration from those tested, since in glass objects the stress at failure is strictly related to the extension of the surface subjected to tensile stress. On the contrary, the Weibull parameters can also be used for the determination

Table 2 Weibull module (β) and Weibull characteristic parameter (σ_0) for Schott D263 glass plates examined in the present work. The minimum tensile stress σ_{min} at breaking point is also reported.

Specimens set	β	σ_0 (MPa mm$^{2/\beta}$)	σ_{min} (MPa)
TQ	6.7	597.9	117
STEEL	4.3	612.8	43
GLASS	4.6	595.0	53
MOULD	4.8	488.1	76
AIR-P$_{air}$	5.0	926.4	90
AIR-P$_{mold}$	4.7	597.5	74
AIR-C$_{air}$	5.7	419.9	110
AIR-C$_{mold}$	6.3	241.2	82
Laser cut[a]	3.39	674.1	76

[a]SET composed by 50 samples previously tested to check laser cutting effects on glass edge strength[45] and whose results have been included in the following.
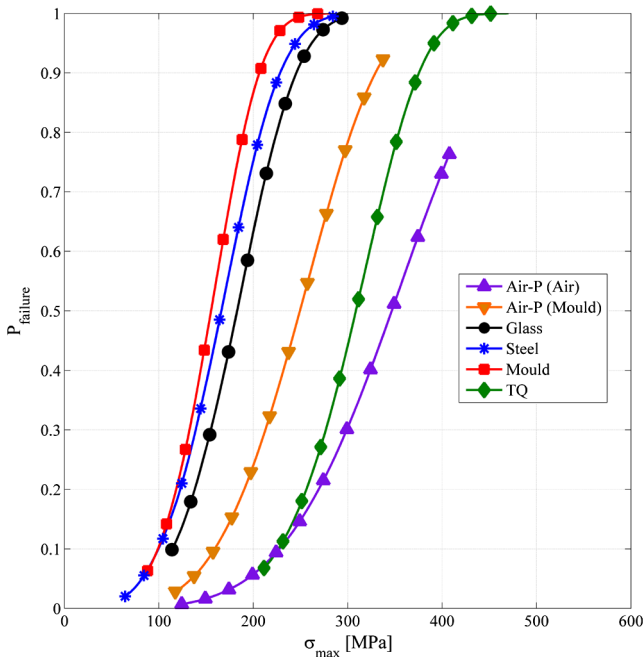
Fig. 15 Comparison of the Weibull curves, i.e., fracture probability of the glass plates versus the maximum value of principal tensile stress, obtained for the different sets of flat samples.

of the failure probabilities for different geometries and loads combinations.

The experimental results show the differences between untreated specimens (set TQ) and the slumped glass foils. This is immediately observable on Fig. 15, in which the fracture probability of the glass samples versus the maximum value of the principal tensile stress is plotted. It appears clear that the slumping process affected the characteristic strength of glass, i.e., lowering it. An improvement in the characteristic strength has been obtained with the new slumping approach. Indeed, the failure probability curves for samples AIR-P appear to be closer to that of the glass foils as delivered by the vendor (TQ), suggesting the possibility of maintaining a good strength of the glass by controlling the glass-mold contact during the slumping process and all related phases of handling and storage. The strength of the set AIR-P$_{air}$ was higher than that of the untreated glass (a lower failure probability); this contradicting result may be due to the relative low number of specimens on which the pertinent Weibull parameters relied. More accurate results can be obtained by increasing the number of specimens. It is worth noting that the breakage stresses for flat and curved specimens are not directly comparable since they were obtained from different testing setups. In the experimental data range, the lower tail of the failure probability distribution proved to be overestimated. This effect, particularly evident for sets STEEL and GLASS, is most likely due to the presence of a nonhomogeneous defect on the glass surface, as evidenced by the quite disperse stress values at breakage that justify the low values for the Weibull modulus (4 ÷ 4.5).

5 Application of Results to IXO Case

The first application of the results was the assessment of the current design of the IXO x-ray telescope.

5.1 Current IXO X-Ray Telescope Design Based on Slumped Plates

The major requirements for the IXO x-ray telescope are a collecting area of around 2.5 to 3 m^2 at 1.25 keV with a 5-in. angular resolution. These can be fulfilled with a Wolter I telescope of 20-m focal length and comprising 350 mirror shells with a radius of curvature ranging from 0.3 to 1.7 m. The current design requires 16,560 glass mirror segments, stacked into basic modules (XOU) through the use of glass spacers between segments of consecutive coaxial shells (ribs) and comprising two glass elements (back and front planes) which gives stiffness to the entire structure.[8] Two hundred XOUs are arranged in eight rings and eight petals to fill the available geometric area of the telescope and to re-establish the cylindrical symmetry of the nested Wolter I optical design. The current XOU configuration, reported in Fig. 16, is representative of an intermediate module belonging to ring 5 and composed of 40 plate pairs with an average radius of curvature of 1000 mm. The connecting ribs have the same length as the mirror foils, i.e., 200 mm, and are bonded to the mirror foils along their whole length: they accomplish the twofold function of keeping the mirror segments in shape and in their relative positions while guaranteeing structural support for them.

The XOUs and IXO telescope design have been supported by a large set of FEA carried out on proper material models with the commercial software Ansys. Lacking a system level study specifically dedicated to the adoption of slumped glass technology for IXO units, reference mechanical and thermal environments have been retrieved from specifications relevant to silicon pore optics technology, with some adjustment justified by the larger XOU mass when compared with a single silicon pore optics module.[19]
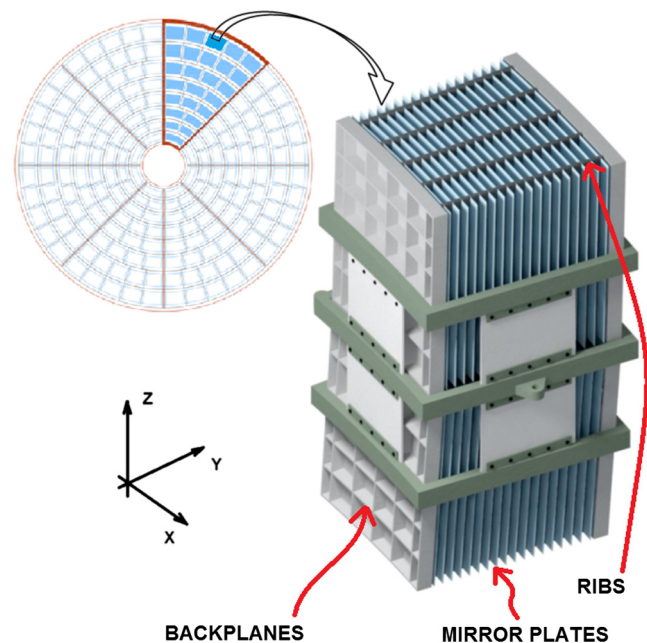

Fig. 16 Conceptual design of the flight mirror assembly (FMA). The x-ray optical units (XOUs) are arranged in eight ring and eight petals. The current design of an intermediate XOU is also shown, with indication of the adopted reference system for the considered loading conditions.

In the absence of any experimental data, an ultimate deterministic glass strength, in terms of maximum loads that can be sustained without breaking the mirrors, was stated and adopted during the design of all glass components: the allowable reference strength, derived from experience and literature, was assumed at the beginning to be equal to 6.7 MPa for long lasting loads and 10 MPa for short lasting and impulse loads. After this study, we can rely on experimental data to check the goodness of this hypothesis. The statistical strength distributions inferred from the experiment can be applied to relate the stress field that builds up inside the mirror segments (due to the load at which the optical payload is subjected) to their survival probability.

The current analysis takes into account only one failure mechanism, i.e., the mirror foils' failure. Other glass elements (i.e., ribs and backplanes) have not been considered yet since available methods for strength improvements can be applied during their production such as, for example, chemical etching, fire polishing or tempering. That would include all methods whose application to mirror segments is not straightforward and needs to be developed in order to preserve their precise optical shape.

5.2 Assessment of the Structural IXO Telescope Design

To check the goodness of the current IXO structural design, the first step was to apply Eq. (4) to derive the survival probability of any single plate of any XOU when subjected to the stress field generated by load conditions.

Simplifying hypotheses has been introduced for representing the loadings: only equivalent static loads and acoustic pressure at launch are considered since they represent the worst case for satellite payloads. In practice, the survival probabilities have been computed for the higher stress level (i.e., the one which gives the maximum failure probability) generated by the vectorial combination of equivalent static loads at launch (± 70 g longitudinal direction and 55 g lateral direction) plus an equivalent acoustic pressure (simulated by applying a ± 66 g load in the radial direction and in addition to the quasi static loads just on the mirror foils). Also, a bulk temperature variation at launch (equal to $\Delta T = \pm 20°C$ for the conservative case) has been assumed (see Ref. 46 for further details on loading conditions).

The Weibull parameters evaluated by SSV are relevant to the case of biaxial stresses, with equal principal tensile stresses. In this case, the risk of failure is independent of flaw orientation, because a flaw of any orientation is exposed to the same stress. Instead the stress fields computed in the mirror foils by FEA are, obviously, unequal principal stresses and this reduces the risk of failure. This effect is taken into account by introducing a biaxial stress correction factor according to the approach presented in Ref. 41. This represents a step forward with respect to a previous work realized by NASA,[14] in which no corrective factor was applied. The correction factor, as clearly visible in Fig. 17, depends on the ratio between the minimum and the maximum principal stresses at each point (σ_I and σ_{II} being σ_I the maximum tensile stress, >0) and on the Weibull module β. It is computed with the hypothesis that all crack locations and orientations have the same probability of occurrence and that individual flaws do not influence each other. In addition, the evaluated parameters have been normalized taking into account the
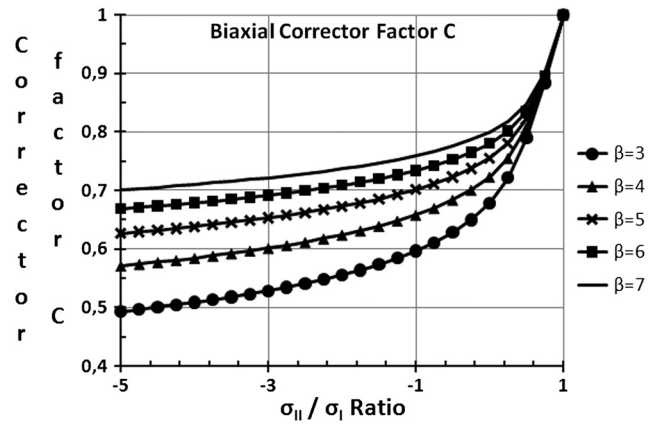

Fig. 17 Correction factor taking into account nonuniform biaxial stress reported as a function of the ratio between the two principal stresses σ_I and σ_{II} (where σ_I is the maximum tensile stress >0) and in dependence of different values of the Weibull modulus β.

effective extension of the surface subjected to the tensile load (integration on foil surface A in the equation).

The survival probabilities related to each surface of any of the mirror plates (i.e., front, back, or edges) have been considered separately in order to discern the surface that has the higher failure risk. To consider the effects of edges, the results of a previous test campaign as reported in Table 2 have been employed.[45] The surface having the higher failure risk was then considered for the computation of the cumulative survival probability of a whole XOU composed of 40 plate pairs. The last step was the estimation of the survival probability of the whole FMA relying on the hypothesis that all 200 XOUs present the same survival probability (in principle, it could be different since the eight different types of XOUs in the FMA could be subjected to different input loads; however, as a first approximation, they are all considered identical). The effect of static fatigue has not taken into account in this first approach to the problem.

These steps have been performed for four cases, both with or without considering the effect of edges:

- Case 1 is representative of the best condition achievable in the unrealistic case where slumping process and related activities do not reduce the mirror plates' strength at all (use of Weibull parameters from set TQ).
- Case 2 is representative of the impact on the glass plate's strength related to the initial slumping approach with a metal membrane to apply pressure (use of Weibull parameters from sets STEEL and MOULD).
- Case 3 is representative of the current new slumping process without the use of the metal pressing membrane, as evaluated with flat samples (use of Weibull parameters from sets AIR-P_{air} and AIR-P_{mold}).
- Case 4 is representative of the current new slumping process without the use of the metal pressing membrane, as derived from cylindrical samples (use of Weibull parameters from sets AIR-C_{air} and AIR-C_{mold}).

A major important hypothesis assumed in the analyses concerns the definition of a catastrophic failure. The evaluation of the consequences in case 1 or if several mirror plates

break is not a trivial task and it would require engineering activities at the system level. So at the moment, we rely on the very severe assumption that the breakage of just 1 out of the 16,560 mirror plates, which compose the whole FMA, determines a catastrophic failure, i.e., could lead to the complete mission failure. In other words, in order to avoid catastrophic breakage, it has been required that no one among the 16560 mirror foils of the FMA crashes, which can probably be considered a worst case scenario.

The results suggest that the glass foil material in condition "as delivered" guarantees a survival probability at the FMA level of 99.999% when the possibility of failure at the edges is excluded, and of 99.23% when failure at the edges is taken into account. A relevant worsening of the strength, both on optical and back mirror surfaces, is recorded after the application of the "old standard slumping process." In this case, in fact, failure probability is increased by a factor of 12,000 at the optical surface and of 39,000 at the back surface, with a drop in the survival probability of FMA to 79.60 or 80.22% if failure at edges is excluded. The general worsening masks the impact of the breakage at the edges. The situation is greatly improved when considering the "new slumping process." The failure probability at the optical front surface is almost confirmed, but the back surface strength gains two orders of magnitude with respect to the previous case, resulting in a survival probability at the FMA level equal to 96.27 or 97.02% if failures at the edges are excluded. The result is confirmed for flat and cylindrical samples, with only minor statistical differences. The results are promising and suggest that, under the considered hypotheses, the level of 99% survival probability of the FMA mirror plates seems achievable with the present XOU design, with only minor optimization of the slumping technique and an improvement of the cutting phase. Furthermore, in order to increase the survival probability of the mirror segments assembly, the possibility of realizing a procedure by scanning and/or by load tests for a preliminary proof test to be applied to the mirror plates before integration should be considered in order to identify the weak plates that need to be discarded.

We are aware of the limitations of the presented analysis: the reliability of the Weibull parameters describing the mirror plates strength is affected by the relatively scarce number of specimens available and the statistical strength distributions suffer from the smallness of the tested area in comparison to the total surface of the FMA mirror plates. At the moment, each specimen allows for the assessment of a few square centimeters of surface while the number of glass foils in the FMA reaches much larger areas (around 1200 m^2). The adopted two-parameter Weibull approach assumes that all stress levels, even very low ones, contribute to the failure probability. So, even with very low stresses, for large stressed areas as in our case, there is a not-negligible failure probability. In this regard, this approach could become too severe and we think a three-parameter Weibull function should be adopted for future activities. Furthermore, the Weibull distribution is applied outside the range of the experimental values, on the lower tail of the probability distribution, in a zone where no experimental evidence about the representation of their real statistical strength distribution exists. The feeling is that the distribution obtained could be particularly severe when extrapolated to the stress level envisaged in the mirror plates (see Ref. 47). This feeling is also supported by simple

evaluations based on a linear fracture mechanic. The flaws' size at failure has been evaluated as a function of the tensile stress acting in a direction normal to the surface defect, according to the linear fracture mechanic criteria and assuming a fracture toughness of $K_{IC} = 0.75$ MPa m$^{1/2}$ for the mirror foil material.[41] It appears that, at the stress level assumed for the XOU design, quite large cracks are necessary to trigger glass failure. In the case of through thickness cracks, the failure flaw size is in the range 2.5 to 3 mm; while for "thumbnail" cracks, stresses considerably larger (at least a multiplying factor 2.5 to 3) than those assumed in design phases are necessary in order to activate the failure, starting from initial cracks 1 to 4-mm long and 0.25 to 0.6-t deep (t = mirror foil thickness).

Despite these limitations, this preliminary approach to the problem represents an important step forward in the comprehension of the slumping technique and gave us the possibility for looking deeply inside some phases of the slumping process and its related activities, indicating the direction for achieving optimization.

6 Conclusion

The surface strength of glass after the application of a slumping thermal-pressure cycle has been evaluated through double-ring destructive tests. More than 200 specimens have been tested to take into account the effect of the "old slumping process" (in which the pressure was applied through a metal membrane) or of the "new slumping process" (in which pressure is directly applied on the glass foil). All samples have been realized following all the steps (except coating deposition and integration) envisaged for the final mirror segments, using the best current knowledge of the process. In particular, 0.4-mm-thick D263 glasses have been slumped on Zerodur K20 and cut to dimensions of 100 mm × 100 mm, as required for the double-ring tests. The recorded empirical values have been compared with nonlinear finite element analyses to derive the stress field in the glasses at breaking. A statistical analysis allowed for the determination of the Weibull parameters of glass, which gives the failure probability associated with a particular stress value. The first application of the derived parameters consisted of a reliability assessment of the current IXO structural design. Present results are promising and suggest that the level of 99% survival probability of the mirror foils of the whole FMA under equivalent static loads seems reachable with the present XOU design (considering that only minor improvements in the slumping technique and an optimization of the cutting technology, despite the strength reduction of the glass after slumping, mainly comes from surface damages due to the contact between glass and other materials employed during the mirrors' manufacturing).

References

1. C. J. Hailey et al., "Fabrication and performance of Constellation-X hard x-ray telescope prototype optics using segmented glass," *Proc. SPIE* **5168**, 90–99 (2004).
2. M. Ghigo et al., "The manufacturing of the XEUS x-ray glass segmented mirrors: status of the investigation and last results," *Proc. SPIE* **5168**, 180–195 (2004).

3. M. Ghigo et al., "Slumped glass option for making XEUS mirrors: preliminary design and ongoing developments," *Proc. SPIE* **7011**, 70111F (2008).
4. M. Skulinova et al., "New light weight x-ray optics—alternative materials," *Proc. SPIE* **7360**, 736016 (2009).
5. M. Vongehr et al., "Development of slumped glass mirror segments for large x-ray telescopes," *Proc. SPIE* **7011**, 701115 (2008).
6. J. Bookbinder, "An overview of the IXO Observatory," *Proc. SPIE* **7732**, 77321B (2010).
7. N. Rando et al., "Status of the ESA L1 mission candidate ATHENA," *Proc. SPIE* **8443**, 844328 (2012).
8. M. Civitani et al., "IXO x-ray mirrors based on slumped glass segments with reinforcing ribs: optical and mechanical design, image error budget and optics unit integration process," *Proc. SPIE* **7732**, 773242 (2010).
9. W. W. Craig et al., "Fabrication of the NuSTAR flight optics," *Proc. SPIE* **8147**, 81470H (2011).
10. F. A. Harrison et al., "The nuclear spectroscopic telescope array (NuSTAR) high-energy x-ray mission," *Astrophys. J.* **770**(2), 103 (2013).
11. N. F. Brejnholt et al., *The Rainwater Memorial Calibration Facility for X-Ray Optics*, Vol. 2011, Article ID 285079, 9 pages, Hindawi Publishing Corporation X-Ray Optics and Instrumentation (2011).
12. W. W. Zhang et al., "Mirror technology development for the international X-ray observatory mission (IXO)," *Proc. SPIE* **7732**, 77321G (2010).
13. M. Ghigo et al., "Development of high angular resolution x-ray telescopes based on slumped glass foils," *Proc. SPIE* **8443**, 84430R (2012).
14. C. He and BATC et al., "Constellation-X: glass strength investigation for SXT, Constellation-X: BATC," Memorandum No. MEB-2008-010 dated 3-25-2008 (2008).
15. G. Pareschi et al., "IXO glass mirrors development in Europe," *Proc. SPIE* **8147**, 81470L (2011).
16. M. J. Collon et al., "Design, fabrication, and characterization of silicon pore optics for ATHENA/IXO," *Proc. SPIE* **8147**, 81470D (2011).
17. ATHENA Assessment Study Report (Yellow Book), "ATHENA: The extremes of the Universe: from black holes to large-scale structure," http://sci.esa.int/athena/49835-athena-assessment-study-report-yellow-book/# (2012).
18. M. M. Civitani et al., "Accurate integration of segmented x-ray optics using interfacing ribs," *Opt. Eng.* **52**(9), 091809 (2013).
19. G. Parodi et al., "Design of the IXO optics based on thin glass plates connected by reinforcing ribs," *Proc. SPIE* **8147**, 81470Q (2011).
20. A. Winter, M. Vongehr, and P. Friedrich, "Light weight optics made by glass thermal forming for future X-ray telescopes," *Proc. SPIE* **7732**, 77320B (2010).
21. L. Proserpio et al., "Production of the IXO glass segmented mirrors by hot slumping with pressure assistance: tests and results," *Proc. SPIE* **8147**, 81470M (2011).
22. M. Ghigo et al., "Slumping technique for the manufacturing of a representative x-ray grazing incidence mirror module for future space missions," *Proc. SPIE* **8884**, 88841Q (2013).
23. EN 1288-1:2000, Glass in building—"Determination of the bending strength of glass—Part 1: Fundamentals of testing glass," CEN (2000).
24. EN 1288-2:2000, Glass in building—"Determination of the bending strength of glass—Part 2: Coaxial double ring test on flat specimen with large test surface area," CEN (2000).
25. EN 1288-3:2000, Glass in building—"Determination of the bending strength of glass—Part 3: Test with specimen supported at two points (four-point bending)," CEN (2000).
26. EN 1288-5:2000, Glass in building— "Determination of the bending strength of glass—Part 5: Coaxial double ring test on flat specimen with small test surface area," CEN (2000).
27. R. Dall'Igna, A. D'Este, and M. Silvestri, "Comments on test methods for the determination of structural glass strength," in *XXV A.T.I.V. (Association of Italian Glass Technologists)*, Parma, Italy (2010).
28. ASTM C 158-02, *Standard Tests Methods for Strength of Glass by Flexure (Determination of Modulus of Rupture)*, American Society for Testing Materials (2008).
29. M. H. Krohn et al., "Strength and fatigue of float glass before and after enameling," *Glass Researcher* **11**(2), 24–28 (2002).
30. A. A. Wereszczak et al., "Size scaling of tensile failure stress in float soda-lime-silicate glass," *Int. J. Appl. Glass Sci.* **1**(2), 143–150 (2010).
31. B. Salmaso et al., "Micro-roughness improvement of slumped glass foils for x-ray telescopes via dip coating," *Proc. SPIE* **8861**, 88610W (2013).
32. A. G. Evans, "A general approach for the statistical analysis of multiaxial fracture," *J. Am. Ceramic Soc.* **61**(7–8), 302–308 (1978).
33. S. B. Batdorf and H. L. Heinisch Jr., "Weakest link theory reformulated for arbitrary fracture criterion," *J. Am. Ceramic Soc.* **61**(7–8), 355–358 (1978).
34. S. B. Batdorf and G. Sines, "Combining data for improved Weibull parameter estimation," *J. Am. Ceramic Soc.* **63**(3–4), 214–218 (1980).
35. D. K. Shetty et al., "A biaxial-flexure test for evaluating ceramic strengths," *J. Am. Ceramic Soc.* **66**(1), 36–42 (1983).
36. L. Y. Chao and D. K. Shetty, "Equivalence of physically based statistical fracture theories for reliability analysis of structural ceramics in multiaxial loading," *J. Am. Ceramic Soc.* **73**(7), 1917–1921 (1990).
37. A. Bruckner-Foit et al., "Discrimination of multiaxility criteria using brittle fracture loci," *J. Eur. Ceramic Soc.* **16**(11), 1201–1207 (1996).
38. W. Weibull, "A statistical distribution function of wide applicability," *J. Appl. Mech.* **18**, 293–297 (1951).
39. D. Munz and T. Fett, *Ceramics. Mechanical Properties, Failure Behaviour, Materials Selection*, pp. 181–189, Springer, Berlin, Heidelberg, New York (1999).
40. W. L. Beason, *A Failure Prediction Model for Window Glass, Institute for Disaster Research*, Texas Tech University Press, Lubbock, Texas (1980).
41. W. L. Beason and J. R. Morgan, "Glass failure prediction model," *J. Struct. Eng.* **110**(2), 197–212 (1984).
42. ASTM C 1239-06A, *Standard Practice for Reporting Uniaxial Strength Data and Estimating Weibull Distribution Parameters for Advanced Ceramics*, American Society for Testing Materials (2004).
43. Glass in building. Procedures for goodness of fit and confidence interval for Weibull distributed glass strength data, EN 12603:2002.
44. Standard practice for reporting uniaxial strength data and estimating Weibull distribution parameters for advanced ceramics, ASTM C1239-06A.
45. Internal document: Resistenza meccanica del bordo di lastre di vetro boro-silicato, Report SSV N.92372—23/12/2009.
46. ESA contract 22545 document: IXO PROJECT—Design of a X-ray Optical Unit using glass mirrors, IXO-BCV-RE-002—Issue 1—29/9/2011.
47. Internal document: Resistenza meccanica di lastre Schott D263 lavorate a caldo, Report SSV N.108932—7/5/2013.

Biographies of the authors are not available.